Bull Math Biol (2014) 76:1917–1940
DOI 10.1007/s11538-014-9991-1

Society for Mathematical Biology

ORIGINAL ARTICLE

Microtubule Patterning in the Presence of Stationary Motor Distributions

Diana White · Gerda de Vries · Adriana Dawes

Received: 21 October 2013 / Accepted: 24 June 2014 / Published online: 18 July 2014

Abstract In this paper, we construct a novel nonlocal transport model that describes the evolution of microtubules (MTs) as they interact with stationary distributions of motor proteins. An advection term accounts for directed MT transport (sliding due to motor protein action), and an integral term accounts for reorientation of MTs due to their interactions with cross-linking motor proteins. Simulations of our model show how MT patterns depend on boundary constraints, as well as model parameters that represent motor speed, cross-linking capability (motor activity), and directionality. In large domains, and using motor parameter values consistent with experimentally-derived values, we find that patterns such as asters, vortices, and bundles are able to persist. In vivo, MTs take on aster patterns during interphase and they form bundles in neurons and polarized epithelial cells. Vortex patterns have not been observed in vivo, however, are found in in vitro experiments. In constrained domains, we find that similar patterns form (asters, bundles, and vortices). However, we also find that when two opposing motors are present, anti-parallel bundles are able to form, resembling the mitotic spindle during cell division. This model demonstrates how MT sliding and MT reorientation are sufficient to produce experimentally observed patterns.

Keywords Microtubules · Motor proteins · Pattern formation · Non-local model

Electronic supplementary material The online version of this article (doi:10.1007/s11538-014-9991-1) contains supplementary material, which is available to authorized users.

D. White (✉) · G. de Vries
University of Alberta, Edmonton, AB, Canada
e-mail: dtwhite@ualberta.ca

A. Dawes
Ohio State University, Columbus, OH, USA

1 Introduction

Understanding how microtubules (MTs) organize in space, and how they undergo transitions between different structural configurations, is crucial to understanding normal cell function. For example, in most non-dividing cells (cells in interphase), MTs take on an astral configuration (see Fig. 1a) (Yuko 2001). Such a configuration provides structural support for the cell, and provides a means of transporting important proteins throughout the cell (via directed transport by motor proteins). In dividing cells, MTs are organized into two astral patterns at the cells centrosomes, with a tight anti-parallel bundle of MTs located between the centrosomes (see Fig. 1b). In most cells, MT organization can be characterized by one of four distinct patterns (or combinations thereof): asters, anti-parallel bundles, parallel bundles, and bundles of mixed polarity (see Fig. 1a–d, respectively) (Dogterom and Surrey 2013).

Understanding the components involved in MT organization is a problem of broad scientific interest. In the last decade, imaging techniques have advanced to the point where it is possible to track individual MTs in space and time. Now, it is possible to test mathematical models by comparing theoretical results with experimental results. In fact, many theoretical models have been developed to describe MT patterns formed through interactions with motor proteins, and qualitative results compare favorably to results found in experiment (Kim et al. 2003; Lee and Kardar 2001; Aranson and Tsimring 2006; Jia et al. 2008). However, a model describing a broad range of patterns found in cells, or one that quantitatively describes the mechanisms involved in patterning, has not yet been developed, and so this is the focus of our paper.

MTs are dynamic protein polymers formed through the self-assembly of α-, β-tubulin dimers (Karp 1996; Wade 2009). They grow through the addition of GTP-bound tubulin dimers, generally from the plus end of the MT (the end containing the majority of β-tubulin), and shrink through dissociation of GDP-bound tubulin at this end. The minus end of the MT (the end where the majority of α-tubulin is located), is generally more stable, being capped by stabilizing proteins. However, MTs can shrink through dissociation of tubulin dimers at this end when such capping proteins are missing. Two primary types of dynamic movement that MTs undergo are treadmilling

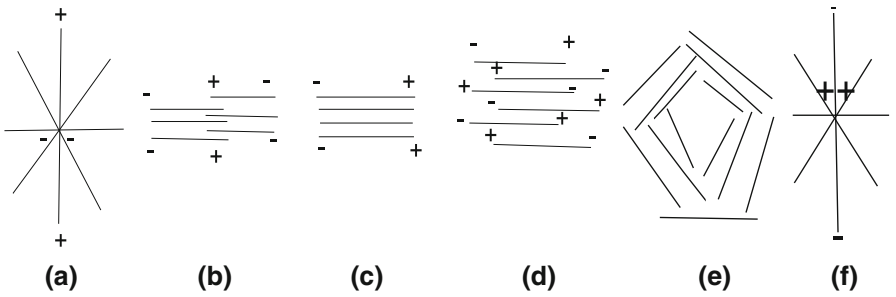

Fig. 1 Examples of MT organization in vivo and in vitro. In vivo organizations include **a** an *aster* with *minus ends* at the center (typical of a centrosomal configuration found in non-dividing cells), **b** an anti-parallel bundle (similar to the mitotic spindle of a typical dividing cell), **c** parallel bundles (similar to those along the axon of a neuron), and **d** mixed polarity bundles (similar to those found in plant cells). In vitro examples include those described in **a**–**d**, but also include **e** vortices, and **f** an *aster* with *plus ends* at the center

(Waterman-Storer and Salmon 1997; Mitchison and Kirschner 1986) and dynamic instability (Kirschner and Mitchison 1984; Waterman-Storer and Salmon 1999). MT treadmilling is a chemical process that is defined as the steady-state unidirectional flux of subunits through a polymer as a result of continuous net assembly at one end of a polymer and continuous net disassembly at the other end. The total result is the directed (constant) motion of the MT towards its plus end. Treadmilling has been observed in vivo, but is often hard to reproduce experimentally. Dynamic instability refers to slow growth of a MT at its plus end, followed by fast depolymerization, and has been observed both in vivo and in vitro. In this study, we focus on comparing our MT patterning results to in vitro results (Nedéléc et al. 1997; Surrey et al. 2001) where treadmilling is not observed, and so we neglect MT treadmilling. Also, for simplicity, we focus on the effects of motors on MTs of constant length (stabilized MTs), and so the primary model presented in this paper (in Sect. 2) is independent of MT growth dynamics.

MT patterning not only depends on the dynamic properties of MTs, it also depends on many other factors, some of which include the spatial constraint of the boundary, as well as MT–MT interactions mediated by motor proteins. For example, Vignaud et al. demonstrate that local effects at the boundary can propagate throughout the domain, changing the qualitative organization of MTs (Vignaud et al. 2001). Also, in some types of cells, such as fission yeast cells, motor proteins are a primary contributor to MT astral organization (Janson et al. 2007). In fact, in the past few decades, in vitro studies (Nedéléc et al. 1997; Nedéléc and Surrey 2001; Surrey et al. 2001; Dogterom and Surrey 2013) have shown that, in systems comprising of only MTs and motor proteins, MTs can organize into many different types of patterns, like those described above in Fig. 1a–d, and also newer patterns not found in vivo, like vortices and asters with plus ends at the aster center (see Fig. 1e, f, respectively).

Motor proteins are ATPases, and so are driven by the hydrolysis of adenosine triphosphate (ATP). By transforming chemical energy into work, they are able to perform a number of important functions. One function of many motors is that they are able to walk along MTs (either towards their plus end or minus end), carrying important proteins with them, distributing them to the appropriate locations within cells. Motor proteins can also affect MT organization. They can do so by either (1) helping to align MTs parallel with one another by MT cross linking, and/or (2) by aiding in MT-directed transport (MT sliding). MT alignment occurs when motor proteins are cross-linked to two MTs simultaneously (Nedéléc et al. 1997). As they walk along the MTs simultaneously, they produce pushing and pulling forces that help to reorient the MTs (see Fig. 2a). Some motors can walk long distances along MTs (and are called processive), while others may only walk short distances or not at all (these motors are non-processive). MT sliding occurs when a motor is attached (absorbed) to a non-moving substrate at its cargo domain, where its free legs are able to attach to a MT (Yokota et al. 1995; Gibbons et al. 2001). Since the motor remains stationary, it effectively pushes the MT along its own axis as it walks along it. Such a sliding mechanism is often replicated in in vitro experiments, and is referred to as a gliding assay (Yokota et al. 1995; Gibbons et al. 2001; Vale et al. 1992; Tao et al. 2006) (see Fig. 2b). Sliding speed has been found to vary greatly in such experiments because it depends directly on motor speed.

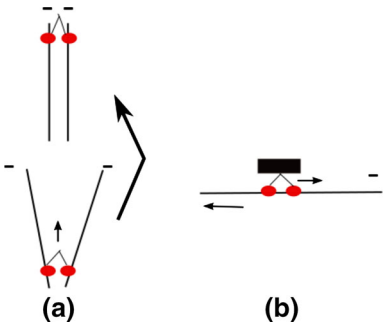

Fig. 2 Examples of MT movement caused by motors. **a** MT reorientation by a minus-end-directed motor, **b** MT sliding

Over the past few decades, both local and non-local models have been proposed to describe how MT patterning occurs in systems composed of motor proteins and MTs. MT *sliding* is described by simple advection (directed movement), placing these models in the category of transport-type models. Transport-type models are defined as models where the particles of interest are defined by their position in space, time, and velocity (Perthame 2007). Defining a model as local or non-local generally has do to with the redistribution part of the model; in our case, this corresponds to MT reorientation (governed by motor proteins). Most models of MT evolution describe MT reorientation using local models (Kim et al. 2003; Lee and Kardar 2001; Jia et al. 2008). Local models incorporate diffusion terms to describe small-scale movement (movement in orientation or location). For example, the model of Lee and Kardar (2001) suggests that MTs undergo small reorientations in the presence of motor proteins. However, we know from recent in vitro studies that large reorientations are possible (Nedéléc et al. 1997; Nedéléc and Surrey 2001), and so non-local models are more desirable from a biological perspective. Non-local models provide a description of large-scale movement and generally use integral terms to describe redistribution. Such non-local models that describe redistribution in terms of probabilities are referred to as velocity-jump models (Othmer 2010), and have a rich history in the study of large-scale animal movement governed by certain cues that can exist over large distances (Othmer et al. 1988). More recently, such models have been used to describe the evolution of cellular systems (Hillen 2006). An interesting example of such a model used in MT/motor systems is a recent study by Aranson and Tsimring (2006). This model uses a diffusion term (to describe small scale fluctuations of MTs in the absence of motors), but also includes a non-local term to describe alignment of MTs as they collide with one another. The action of the motor proteins is implicit here, and suggests that motors are dispersed uniformly throughout space, so that when two MTs interact they instantaneously align due to motor protein action.

Other polymer/motor systems, such as actin/myosin systems, have been studied extensively from both an experimental point of view (Luo et al. 2013; Smith et al. 2007; Humphrey et al. 2002; Reymann et al. 2010) and a theoretical framework point of view. Actin can take on many complex organizations (like MTs), and such organization is crucial for normal cell function. For example, actin forms tight parallel bundles, called filopodia, at the front of fibroblasts, allowing them to migrate in the direction of a wound. Also, during muscle contraction, actin fibers form tight anti-parallel

bundles. Theoretical models have been developed to better understand these and other complex patterns that actin can form when in the presence of myosin. For example, in Miller et al. (2012), the authors use a Monte Carlo modelling approach to model actin movement. They consider both actin rotation (as a result of myosin II motors traversing filament pairs) as well as polymerization and depolymerization of filaments. They find that optimal motor speeds (high speeds) result in alignment of filaments, whereas depolymerization results in disorganized actin structures. To our knowledge, there are no actin models that model polymer sliding and alignment using a similar velocity-jump process similar to what we propose here.

In this paper, we derive a model that uses an advection term to describe MT sliding, as well as a non-local redistribution term that is used to describe MT reorientation in the presence of motor proteins. Our model is different from other non-local models in that there is an explicit interaction of MTs with motors. We define a function that describes MT alignment in terms of cross-linking capability (which we call motor activity). Also, other models have used either parallel or perpendicular-type boundary conditions, forcing MTs to take on particular orientations at the boundary of the domain (Kim et al. 2003). In our model, a novel no-flux boundary condition (which we call the bounce back condition) is used to allow MTs to reorient more naturally at the boundary. Also, other models consider motile motors (Kim et al. 2003; Lee and Kardar 2001; Jia et al. 2008). In general, motors are able to diffuse in the cytoplasm of cells, and can walk along MTs. However, in gliding assay experiments, motors are absorbed to a cover slide (Vale et al. 1992; Tao et al. 2006). In such experiments, motors are stationary, but slide and reorient MTs, reorganizing MTs into various patterns. Therefore, it would be useful to provide a theoretical framework to describe MT patterning in the case where motors are stationary, as we do in this paper. In a separate study, we examine the patterning of MTs in systems of moving motors (White et al. 2014). In vitro experiments have found that MTs can organize into a variety of patterns, including asters, vortices, and bundles, in systems where motors are dynamic (Nedéléc et al. 1997; Surrey et al. 2001).

In Sect. 2, we develop a theoretical model to describe MT evolution by assuming that MT organization is primarily governed by the processes of MT sliding and MT alignment by motor proteins. In Sect. 3, we show results for simulation of our model given in Sect. 2. In particular, in Sect. 3.1, we show that when motors are not able to slide MTs, the model is governed completely by the reorientation process, and the resulting MT patterns are asters or bundles. Then, in Sect. 3.2, we describe MT patterning after long time simulations in the case where MTs slide in the presence of one motor type. Here, we choose to study MT patterning using periodic and bounce-back boundary conditions. For periodic boundary conditions, we compare our results to the experiments of Nedéléc et al. (1997) and Surrey et al. (2001). These experiments are completed in large domains, and so periodic boundary conditions are the most appropriate choice of boundary condition to use to make comparisons. For bounce-back boundary conditions, we compare our results to experiments completed on small domains (Nedéléc et al. 1997). It is interesting to note that motors are not stationary in the experiments of Nedéléc et al. (1997), Surrey et al. (2001). Even though we model motors as stationary, we are still able to make interesting comparisons with experiment. In Sect. 3.3, we describe MT patterning in the case where we have two types of motors

present (motors with opposing directionality). Here, we test both periodic and bounce-back boundary conditions and we compare our results to the gliding assays completed by Vale et al. (1992) and Tao et al. (2006).

2 Modeling MT Evolution in Terms of MT Sliding and MT Alignment by Motor Proteins

In this section, we introduce a new non-local transport model, Eq. (1), that describes how MTs are organized in two-dimensional space by assuming that MTs undergo two primary types of movement: MT sliding and MT reorientation through interactions with motor proteins. In the model, we consider constant length MTs (i.e., we do not consider growth and shortening of MTs through processes such as dynamic instability). Experimentally, MT dynamic instability can be controlled through use of MT stabilizing drugs such as Taxol (Zhou and Giannakakou 2005). In fact, such a drug has been used in previous studies of MT patterning (Nedéléc et al. 1997). Equation (1) describes the evolution of MT density, $p(\mathbf{x}, t, \theta)$, in space $\mathbf{x}$, time t, and orientation θ, as MTs interact with stationary distributions of motors, $m(\mathbf{x})$:

$$\frac{\partial p(\mathbf{x}, t, \theta)}{\partial t} + S_{\text{slide}}\hat{\theta} \cdot \nabla_{\mathbf{x}} p(\mathbf{x}, t, \theta) = -\lambda(m) p(\mathbf{x}, t, \theta) + \lambda(m) \int_{-\pi}^{\pi} k(\theta, \tilde{\theta}, m) p(\mathbf{x}, t, \tilde{\theta}) \mathrm{d}\tilde{\theta}. \quad (1)$$

We consider a domain of size $\Omega = [0, L] \times [0, L]$ with periodic boundary conditions,

$$p(0, y, t, \theta) = p(L, y, t, \theta); \;\; p(x, 0, t, \theta) = p(x, L, t, \theta), \quad (2)$$

or a novel no-flux boundary condition, which we describe numerically in Sect. 2.1. For simplicity in reading, we write $p(\mathbf{x}, t, \theta) = p(x, y, t, \theta)$ in the above boundary conditions.

The left-hand side of Eq. (1) describes how each MT slides with constant speed S_{slide} along its orientation $\hat{\theta} = \begin{pmatrix} \cos(\theta) \\ \sin(\theta) \end{pmatrix}$. We will vary the speed S_{slide} to represent different types of motor proteins (speeds for motor types are given in Table 1). The right-hand side of Eq. (1) describes the interaction of MTs with motors. In particular, when MTs encounter motor proteins, they switch to an orientation θ from an orientation $\tilde{\theta}$ at rate $\lambda(m)$ and with probability $k(\theta, \tilde{\theta}, m)$.

The rate of switching is given by

$$\lambda(m(\mathbf{x})) = \lambda_{\max} \frac{m(\mathbf{x})}{1 + m(\mathbf{x})}, \quad (3)$$

and is a saturating function of the motor protein density, $m(\mathbf{x})$. That is, the more motors present at location $\mathbf{x}$, the higher the switching rate (if there are no motors, there is no MT switching and so $\lambda(0) = 0$). Also, $\lambda(m)$ saturates to a maximal value ($\lim_{m \to \infty}$

$\lambda(m) = \lambda_{\max}$), so that after a particular motor density is reached, MT switching rate will not be affected.

The probability that a MT switches orientation is given by the probability density function $k(\theta, \tilde{\theta}, m)$. We can define k in a number of different ways, however, based on what we know about MT interactions with motor proteins, and for mathematical ease (see Hillen and White 2014), we choose $k(\theta, \tilde{\theta}, m)$ to be the Von Mises distribution,

$$k(\theta, \tilde{\theta}, m) = \frac{1}{2\pi I_0(\alpha(m))} \exp(\alpha(m)\cos(\theta - \mu)), \tag{4}$$

that is centered around the angle μ, with standard deviation $1/\alpha(m)$, and with normalization constant $\frac{1}{2\pi I_0(\alpha(m))}$, where $I_0(\alpha(m))$ is a modified bessel function of order 0. Also, note that k does not depend on the angle $\tilde{\theta}$ for the following reason. Since k is a probability density function, it has the property that

$$\int_{-\pi}^{\pi} k(\theta, \tilde{\theta}, m)\mathrm{d}\theta = 1. \tag{5}$$

As stated above, $1/\alpha(m)$ is the standard deviation of the probability k. The larger the value of $\alpha(m)$, the sharper the peak of the distribution. Since experimental details are lacking that would allow us to specify $\alpha(m)$, we choose the most biologically reasonable form which is the linear function

$$\alpha(m) = Cm(\mathbf{x}), \tag{6}$$

where $m(\mathbf{x})$ is the motor density at each location $\mathbf{x}$, and C is a constant that describes the ability for a motor to cross-link MTs (we call C the motor activity parameter). The higher the value of C (or motor density), the sharper the peak of the function k and the higher the probability of switching orientation. We will vary C to see how these values affect MT patterning under fixed motor density.

Recall that k is centered around the angle μ. We define $\widehat{\mu}$ to be the mean MT orientation vector at a point so that $\widehat{\mu} = \begin{pmatrix} \mu_x \\ \mu_y \end{pmatrix}$, where

$$\mu_x = \frac{\int_{-\pi}^{\pi} \cos(\theta)\, p(\mathbf{x}, t, \theta)\mathrm{d}\theta}{\int_{-\pi}^{\pi} p(\mathbf{x}, t, \theta)\mathrm{d}\theta}, \tag{7}$$

$$\mu_y = \frac{\int_{-\pi}^{\pi} \sin(\theta)\, p(\mathbf{x}, t, \theta)\mathrm{d}\theta}{\int_{-\pi}^{\pi} p(\mathbf{x}, t, \theta)\mathrm{d}\theta}, \tag{8}$$

and so we can write the scalar angle as

$$\mu = \arctan(\mu_x/\mu_y) + j\pi. \tag{9}$$

Here $j = 0$ if $\mu_x > 0$, $j = -1$ if $\mu_x < 0$ and $\mu_y < 0$, and $j = 1$ if $\mu_x < 0$ and $\mu_y > 0$. The assumption that k is centered around the mean MT orientation μ

Table 1 Table of model parameters

Model parameter	Value	Source
Low sliding speed S_{slide} by kinesin-5	0.04 μm/s	Tao et al. (2006), Howard (2001)
Moderate sliding speed S_{slide} by NCD	0.12 μm/s	Tao et al. (2006), Howard (2001)
High sliding speed S_{slide} by conventional kinesin	0.5–0.8 μm/s	Surrey et al. (2001), Howard (2001)
Activity parameter C	$0.01 < C < 5$	This paper
Maximum switching rate $\lambda_{\max}$	40/s	This paper

allows us to simplify the model mathematically, while keeping the model biologically realistic. In particular, the probability of the reorientation of a MT does not depend on the angle from which the MT came, θ, only on the distance between the mean orientation of MTs, μ, and the angle it reorients to. With this simplification in mind, the model given by Eq. (1) can be written as,

$$\frac{\partial p(\mathbf{x},t,\theta)}{\partial t} + S_{\text{slide}}\hat{\theta}\cdot\nabla_{\mathbf{x}}p(\mathbf{x},t,\theta) = -\lambda(m)p(\mathbf{x},t,\theta) + \lambda(m)k(\theta,m)\int_{-\pi}^{\pi} p(\mathbf{x},t,\tilde{\theta})\mathrm{d}\tilde{\theta}. \tag{10}$$

All model parameters required for simulations of the this model: motor activity C, sliding rate S_{slide}, and the maximum switching rate $\lambda_{\max}$ are summarized in Table 1.

2.1 Set-Up for Numerical Implementation

To simulate the advection part of the model (the left-hand side of Eq. 10), we use a first-order upwind scheme at each location. Advection can occur in any orientation, depending on the MT direction θ. For example, if $\theta = 3\pi/4$, the direction vector $\hat{\theta} = \begin{pmatrix}\cos(\theta)\\ \sin(\theta)\end{pmatrix} = \begin{pmatrix}-0.7071\\ 0.7071\end{pmatrix}$, and we perform upwinding in the negative x direction and upwinding in the positive y direction. To simulate the integral term on the right-hand side of Eq. (10), we use the trapezoid method. All simulations are implemented in Matlab using custom code, using a 60×60 unit spatial grid (each unit $\simeq 1.0$ μm, so we are looking at a medium sized cell of size 60×60 μm^2) and an angular grid between $-\pi$ and π with a step size of $\pi/32$. Simulations are run on smaller angular grids, but show similar results, and so we do not use a stepsize smaller than $\pi/32$.

Figure 3 describes the motor distribution and the initial conditions for MTs. Figure 3a describes a uniform fixed motor distribution where we choose a density of 0.1 μm^{-2}. Figure 3b illustrates the initial MT density, which is chosen to be approximately uniform throughout the entire domain ($\simeq$0.1 μm^{-2}), Fig. 3c illustrates the initial mean MT orientation at each spatial location, and Fig. 3d illustrates the orientational distribution at each spatial location (each MT is assigned a random orientation between π and $-\pi$). Each color represents a different orientation, and the length of the vector is proportional to the density of MTs oriented along that direction. To keep the schematic less clustered, we only

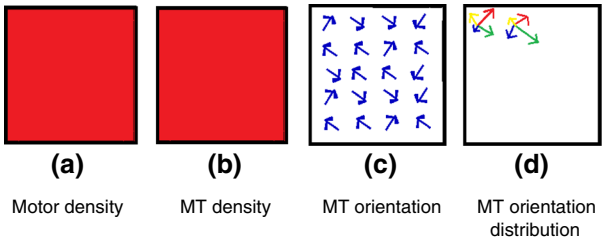

Fig. 3 A schematic of the initial conditions for the model. **a** Motor density is fixed and uniform in space. **b** MT density is initially uniform. *Red* represents high density. **c** Mean MT orientation μ at each point in space. **d** Full MT orientation distribution at each point in space (only two spatial locations shown for clarity) (Color figure online)

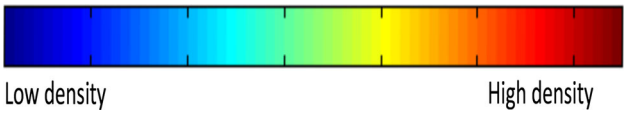

Fig. 4 MT density color bar. In this and all subsequent figures, colors vary from low MT density (*blue*) to high MT density (*red*) (Color figure online)

show four possible orientations, and 20 spatial locations. However, for our simulations, we allow a total of 64 possible orientations for MTs at each spatial location. Figure 4 illustrates MT density, where high MT density corresponds to red and low MT density corresponds to blue (initially, MTs are uniform everywhere in space so the color is red everywhere, as shown in Fig. 3b). As stated in the previous section, we study Eq. (10) using periodic boundary conditions and a novel bounce-back boundary condition. Periodic boundary conditions in two-dimensions are not entirely biologically realistic, since the domain we are effectively describing the movement of MTs on is the two-dimensional surface of a torus, rendering the domain effectively infinite. However, these boundary conditions are generally used for models similar to Eq. (10) because they are relatively easy to simulate, and because they can give insight into MT pattering on large domains. No-flux boundary conditions in two-dimensions are more biologically realistic, since MT movement at the domain boundary is treated similar to how MTs might behave at a cell boundary. No-flux boundary conditions can be difficult to simulate for integral equations such as ours, and so often either parallel or normal boundary conditions are used instead: when a MT (a fixed length rod at a particular orientation) reaches the boundary, it is instantaneously oriented parallel or perpendicular with respect to the boundary (Kim et al. 2003). This boundary condition, though easier to model, does not allow for a natural (smooth) movement of MTs along boundaries. Here, we use a new approach to calculate the orientation of MTs once they reach the boundary, which allows for a more natural movement of the MT. Such a method is described in what follows (see Fig. 5).

Let us just consider the 1D case where we look at only the last few mesh points near the right boundary. Initially, as shown in Fig. 5a, we start with zero MTs on the boundary and one mesh point behind the boundary. During the first half of each time step, we move all MTs according to the appropriate upwind scheme. For simplicity, we just consider an upwind scheme in the right direction, and so all MTs move forward as in Fig. 5b. In Fig. 5c, we show how MTs in the second last mesh point, N, are moved back into the $N-1$ mesh point during the second half of each time step. Now there are zero MTs again

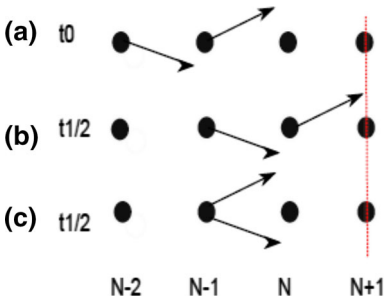

Fig. 5 An example of how bounce back boundary conditions work in 1D for an upwind scheme towards the right direction. **a** We start with zero MTs at the last two mesh points (N and $N + 1$). For simplicity, we choose only one MT per each mesh point, however, in simulations we can have many MTs in each mesh point. At each time step the following two operations are performed: **b** MTs move forward according to the upwind scheme and fill all mesh points, except the last at $N + 1$ (because that is the boundary), **c** MTs in the N mesh point are moved back one mesh point (to $N - 1$), leaving zero MTs in the last two mesh points once again

at the last two mesh points. If we let $p_{j,t,\theta}$ represent the density of MTs at location j, at time t, and orientation θ, we can describe movement of MTs at the boundary during the second half of each time step by,

$$p_{N-1,t+1,\theta} = p_{N-1,t+1/2,\theta} + p_{N,t+1/2,\theta}, \tag{11}$$

$$p_{N,t+1,\theta} = 0. \tag{12}$$

If motors are located at the mesh points defined above, the next step would be to perform reorientation of the MTs according to the integral part of the Eq. (10). However, if motors are not located at these points, the process described in Fig. 5 would be repeated, and the two MTs that are in the $N - 1$ mesh point will move to the N mesh point, but will be moved back into the $N - 1$ mesh point with the MTs that have moved forward from the $N - 2$ mesh point. In effect, we have a build up of MTs on the boundary, since MTs keep being bounced back and forth between the last two mesh points, with new MTs coming in from the $N - 2$ mesh point.

3 Results of MT Patterning in the Presence of Stationary Motors

In this section, we show results of MT patterning under the influence of no motors (Sect. 3.1), one motor type (Sect. 3.2), or two motor types (Sect. 3.3). In both Sects. 3.2 and 3.3, we refer to steady-state patterns as those where the qualitative features of the patterns remain the same after a long time simulation. At the end of this section, we summarize the results for MT patterning in the presence of motors in Tables 2 and 3, corresponding to periodic boundary conditions and bounce-back boundary conditions, respectively.

3.1 Results: Microtubule Patterns for Zero Sliding Speed ($S_{\text{slide}} = 0$)

To gain insight into the dynamics of the model given by Eq. (10), it is useful to first look at a simplified case where the sliding speed, S_{slide}, is zero (there is no spatial movement

Table 2 Summary of results for patterns formed using periodic boundary conditions

	Low C	Moderate C	High C
Kinesin	Vortices	Asters	Bundles
NCD	Asters	Asters	Bundles
Kinesin-5/NCD mixture	Anti-parallel bundles	Mixed	Mixed

Table 3 Summary of results for patterns formed using bounce-back boundary conditions

	Low C	Moderate C	High C
Kinesin	Aster	Vortex	Vortex
NCD	Vortex	Vortex	Vortex
Kinesin-5/NCD mixture	Anti-parallel bundles	Anti-parallel bundles	Anti-parallel bundles

of MTs). Since we are interested in steady-state patterns, we study the time-independent case (where $\frac{\partial p}{\partial t} = 0$). In this case, we arrive at the equation

$$p(\theta) = \int_{-\pi}^{\pi} k(\theta, \tilde{\theta}, m) p(\tilde{\theta}) \mathrm{d}\tilde{\theta}. \tag{13}$$

Such an equation is well studied and is referred to as a Fredholm equation of the second kind (Porter 1990). For our particular choice in k (i.e., for k independent of the previous angle $\tilde{\theta}$), we simplify this equation to

$$p(\theta) = k(\theta, m) \int_{-\pi}^{\pi} p(\tilde{\theta}) d\tilde{\theta}, \tag{14}$$

and since $\int_{-\pi}^{\pi} p(\tilde{\theta}) \mathrm{d}\tilde{\theta}$ is constant, without loss of generality, we can set this constant equal to 1 and so Eq. (14) simplifies to

$$p(\theta) = k(\theta, m). \tag{15}$$

In the limits of α going to zero and infinity we get

$$\lim_{\alpha \to 0} p(\theta) = \frac{1}{2\pi}, \tag{16}$$

$$\lim_{\alpha \to \infty} p(\theta) = \delta(\mu). \tag{17}$$

The set of solution curves for $p(\theta)$, for varying $\alpha(m)$, are shown in Fig. 6.

Recall that the function $\alpha(m) = Cm$, and so if motor density is constant, high α corresponds to high motor activity C, whereas low α corresponds to low motor activity C. The solution curves shown in Fig. 6 show that when MTs are not sliding ($S_{\text{slide}} = 0$), MT organization is entirely defined by the motor activity parameter C. In

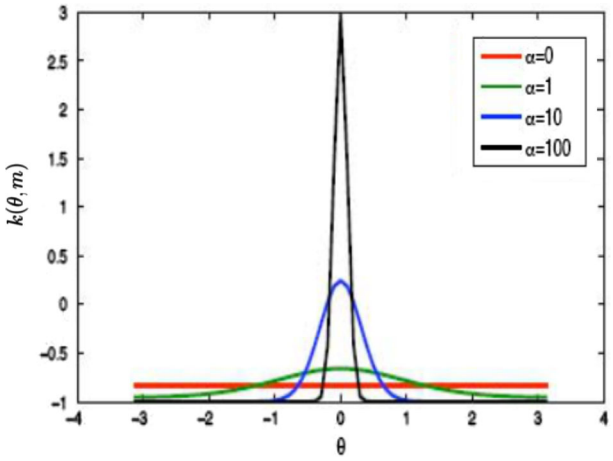

Fig. 6 Solutions for MT distributions given by Eq. (15). Here, $k(\theta, m)$ has mean μ=0 and α = 0, 1, 10, and 100 (Color figure online)

particular, when the motor activity is high, MTs align to a mean orientation μ (form bundles), and when the motor activity is low, MTs take on uniform distributions (form asters).

3.2 Results: Microtubule Patterns for a Single Motor Type (S_{slide} = Constant Everywhere)

In this section, we show simulation results for the full transport model given by Eq. (10) for the case where we have a single motor type that slides MTs. In all cases, we show steady-state patterns. We use motor speeds that are similar to those used in the MT patterning experiments describe in Nedéléc et al. (1997), Surrey et al. (2001). In particular, we choose motor speeds similar to kinesin-1 (conventional kinesin) and nonclaret dysjunctional (NCD) (speeds found in Table 1). We show results for each motor type using either periodic boundary conditions for MTs (Sect. 3.2.1) or bounce-back boundary conditions for MTs (Sect. 3.2.2).

3.2.1 Periodic Boundary Conditions

First, we simulate our model using the conventional kinesin sliding speed (we will call this motor kinesin in what follows). Previous experiments show that in systems comprised of MTs and kinesins, the qualitative patterns of the MTs change from vortex, to aster, to bundled patterns, as you increase the motor density from low to high (Surrey et al. 2001). Results in Fig. 7 correspond to MT patterns for the fast-moving kinesin motor, for varying motor activity C, and using periodic boundary conditions. Recall from Eq. (6), that changes in the value of C have a similar effect to changes in motor density m, with respect the alignment function $\alpha(m)$. From this figure, we see that for fixed motor density (0.1 μm^{-2}), as we increase C, patterns evolve from vortices at low C, to asters at slightly higher C, to a single oriented MT bundle at high C. Changes in MT

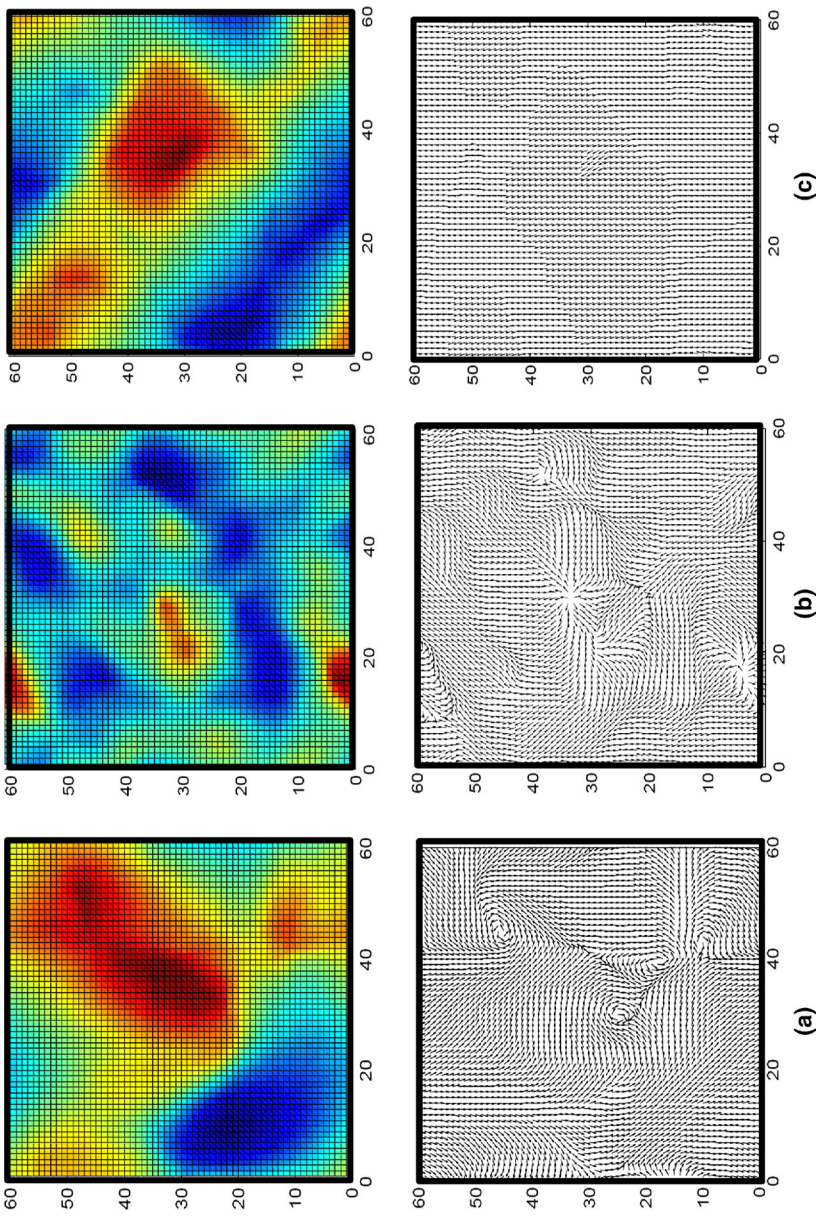

Fig. 7 MT density (*top*) and mean MT orientation (*bottom*) found after large time simulation of MTs under the influence of stationary conventional kinesin motors and using periodic boundary conditions. **a** Vortex patterns found at low $C = 0.01$, **b** aster patterns found for moderate $C = 0.1$, and **c** bundled MTs found for higher $C = 0.5$. *Red* corresponds to a high density of MTs, while *blue* corresponds to a low density of MTs (Color figure online)

density range from low density (blue) to high density (red), and are described by the color bar given in the previous section by Fig. 4. This density color bar applies to all MT density plots that follow. Note that, if we have no motors, we see no bundling (results not shown). However, for non-zero motor density and high C, we do see bundling. This is explained as follows. MTs can switch orientation at any location where a motor is present, and they do so towards the mean MT orientation μ (Eq. 9). At each time step, a MT moving through a motor patch will most likely be aligned to a cluster of MTs that are travelling along the same orientation, and so after large time, MTs tend to cluster together as a group [movie showing single MT bundle formation for high sliding speed S_{slide} (corresponding to kinesin speed), and high motor activity $C = 0.5$ in supplementary materials.]

Next, we simulate our model using the slower NCD sliding speed. Previous experiments show that in systems comprised of MTs and NCD, MTs form aster patterns as you increase the motor density from low to high (Surrey et al. 2001). Figure 8 illustrates results for MT patterning using NCD motors with various motor activities C, and periodic boundary condtions. Here, we see that patterns change from asters at low (to moderate) values of C, to tight bundles at high C. [movie showing aster formation for lower NCD sliding speed S_{slide} and moderate motor activity $C = 0.1$ in supplementary materials.]

3.2.2 Bounce-Back Boundary Conditions

Here, we show results for MT patterning in the presence of either kinesin or NCD motors using bounce-back boundary conditions for MTs. Previous experiments have shown that kinesin can organize MTs into various patterns in small constrained domains (Nedélec et al. 1997). In particular, when kinesin is mixed with stabilized MTs (stabilized by Taxol), MTs form single aster patterns. Also, when kinesin is mixed with dynamic MTs, MTs form vortex type patterns. In Figs. 9 and 10, we illustrate MT patterning in constrained domains using bounce-back boundary conditions. Similar to before, we vary the motor activity C to see how variations affect MT patterning.

Figure 9 illustrates results for a high kinesin sliding speed S_{slide} and for varying C. From this figure, we see that for fixed motor density ($0.1\ \mu\text{m}^{-2}$), as we increase C, patterns evolve from a global aster at low C, to a mixture of vortices at moderate C. Also, as we increase C, the number of MTs located at the center of the domain remains fairly constant, where most MTs end up on the boundary. Even though there is little difference in the MT density patterns, we show all examples to be consistent.

This density pattern is a direct consequence of the bounce-back boundary condition. In particular, only when a MT is oriented towards the boundary can it reach it. At the boundary, a MT can reorient and move in another direction. However, reorientation towards the mean MT orientation (which is directed towards the boundary) is most probable, and so most MTs stay directed towards the boundary and become trapped there. However, there is a small probability that MTs can become oriented away from the boundary and move back into the center of the domain, resulting in a small non-zero MT density at the interior of the domain.

In Fig. 10, we show results for the lower NCD sliding speed S_{slide} and for varying C. Here, we see that patterns change from a very tight vortex at low C to arrays of vortices at higher values of C. [movie showing vortex formation for NCD sliding speed S_{slide} and high motor activity $C = 0.5$ in supplementary materials.]

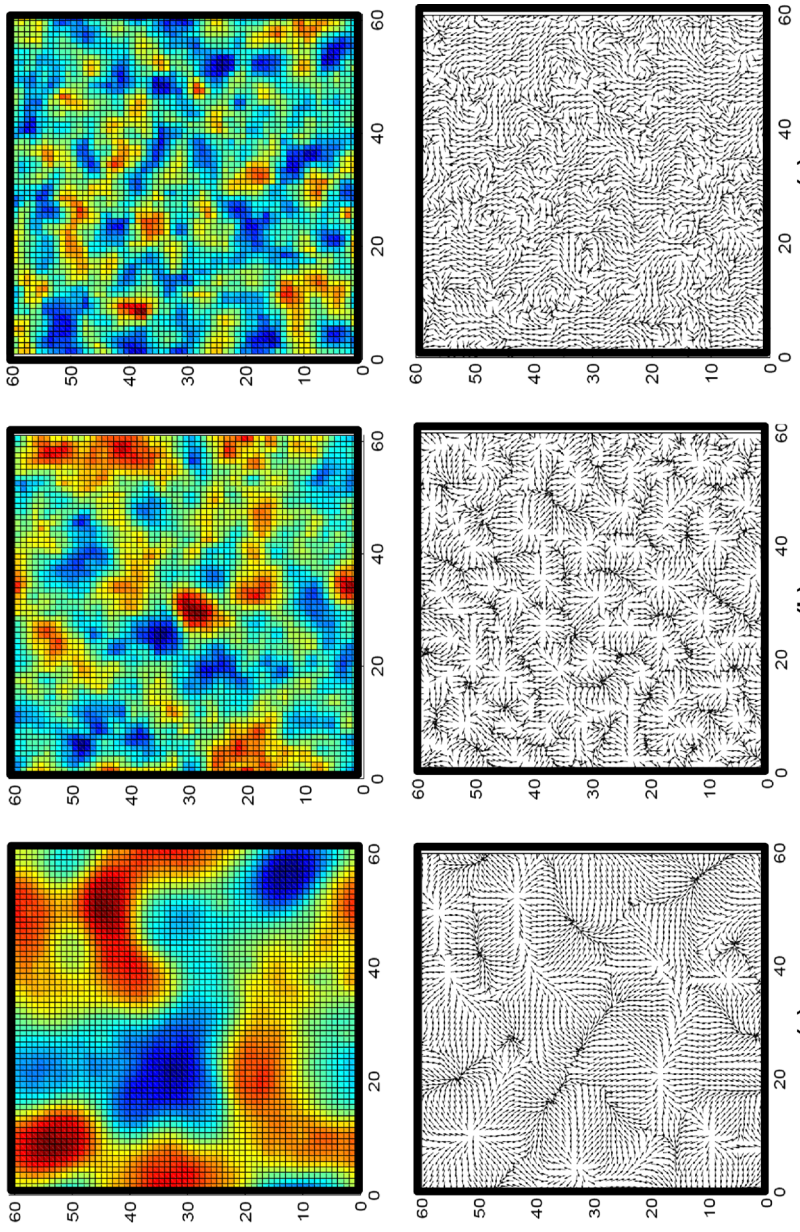

Fig. 8 MT density (*top*) and mean MT orientation (*bottom*) found after large time simulation of MTs under the influence of stationary NCD motors and using periodic boundary conditions. **a** Aster pattern for low $C = 0.01$, **b** aster pattern for moderate $C = 0.1$, and **c** bundled MT pattern for higher $C = 0.5$. *Red* corresponds to a high density of MTs, while *blue* corresponds to a low density of MTs (Color figure online)

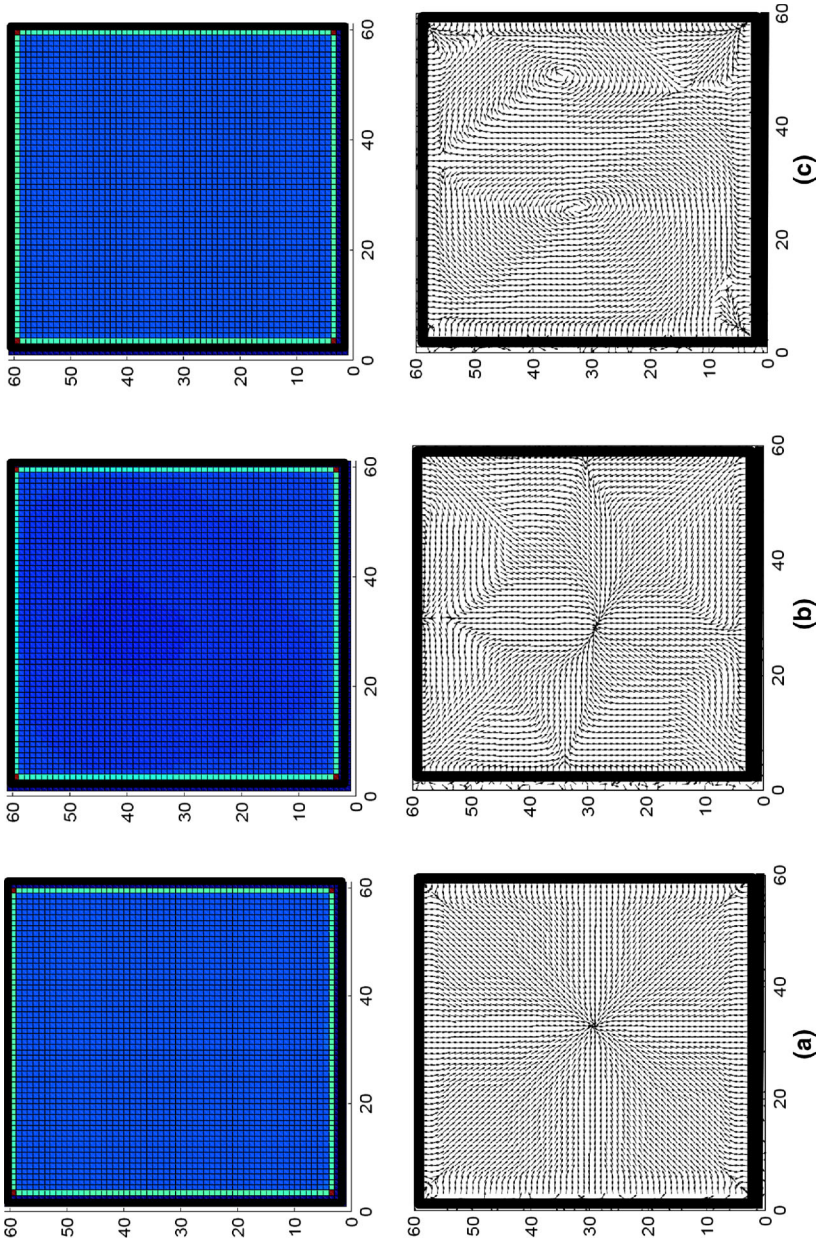

Fig. 9 MT density (*top*) and mean MT orientation (*bottom*) found after large time simulation of MTs under the influence of stationary conventional kinesin motors and using bounce-back boundary conditions. **a** Global aster found at low $C = 0.01$, **b** aster patterns found after short time for moderate $C = 0.1$, and **c** vortex patterns found after long time for moderate $C = 0.1$. *Red* corresponds to a high density of MTs, while *blue* corresponds to a low density of MTs (Color figure online)

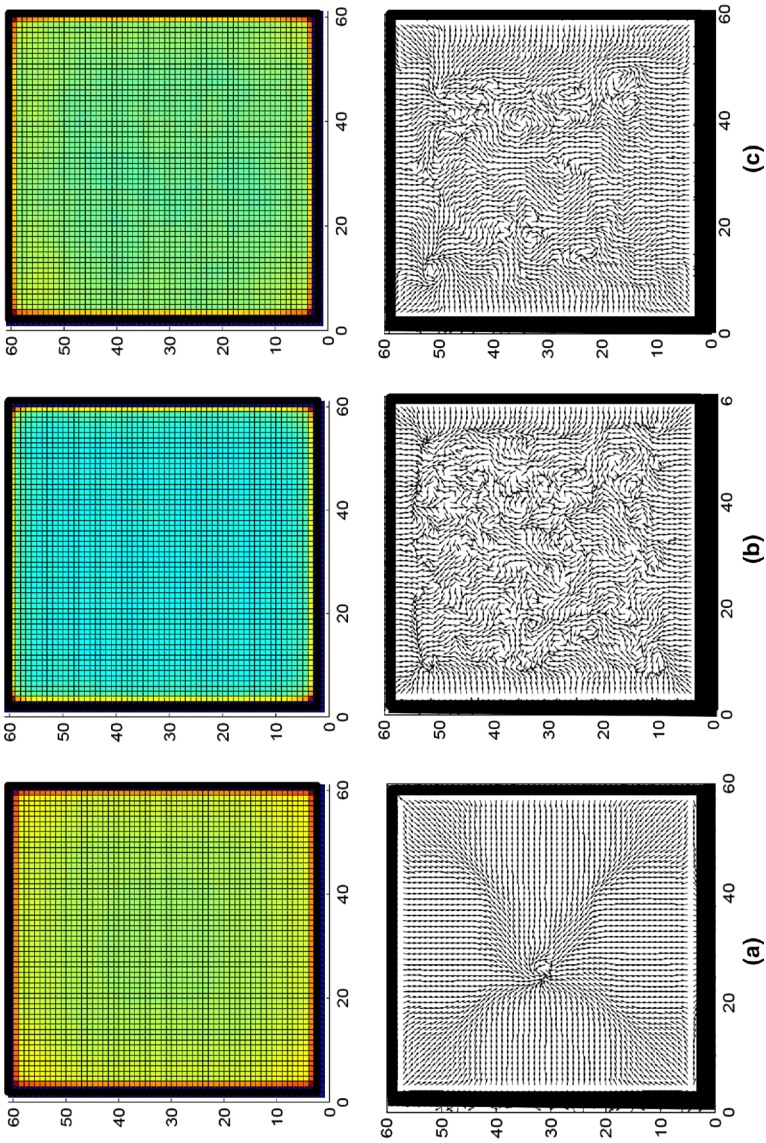

Fig. 10 MT density (*top*) and mean MT orientation (*bottom*) found after large time simulation of MTs under the influence of stationary NCD motors and using bounce-back boundary conditions. **a** Tight global vortex for low $C = 0.01$, **b** vortex patterns found after short time for higher $C = 0.5$, and **c** vortex patterns after long time for higher $C = 0.5$. *Red* corresponds to a high density MTs, while *blue* corresponds to a low density MTs (Color figure online)

For both kinesin and NCD, regardless of speed, for very high C ($C = 25$) most MTs are located at the boundary and the orientation is completely aligned (results not shown).

3.3 Results: Microtubule Patterns for Two Motor Types ($S_{\text{slide}}(x)$ is Not Constant)

In this section, we test how MT patterns can be formed in systems comprised of a mixture of mitotic motors, NCD and kinesin-5. In vivo, NCD is found to be non-processive and fast (speed given in Table 1), whereas kinesin-5 is weakly processive and very slow (speed given in Table 1). Both motors are proposed to generate the antagonistic-sliding forces that control the spacing of the spindle poles and help organize the spindle during cell division. Also, gliding assay experiments have been completed to study how similar motor constructs organize MTs (Vale et al. 1992; Tao et al. 2006). In these experiments, motors are immobile (absorbed to a cover slide) and are found to slide MTs close to their actual walking speed. Here, we test whether such anti-parallel bundles can form by simulating our model using motors with speeds similar to those in the experiment of Tao et al. (2006).

For simplicity, we consider the case where we have an equal number of each motor distributed randomly throughout the entire domain (where the motor density is $0.1\,\mu\text{m}^{-2}$ everywhere). Here, we model the sliding speed as a function of space. In particular, we model the sliding speed in terms of the locations of plus-end (m^+) and minus-end (m^-) directed motors. We define the sliding speed function by

$$S_{\text{slide}}(\mathbf{x}) = S^+_{\text{slide}} \cdot I_{D-}(\mathbf{x}) + S^-_{\text{slide}} \cdot I_{D+}(\mathbf{x}), \tag{18}$$

where S^+_{slide} is the sliding speed of a minus-end directed motor, and S^-_{slide} is the sliding speed of plus-end directed motor (values in Table 1). Here, $I_{D-}(\mathbf{x})$ and $I_{D+}(\mathbf{x})$ are defined by

$$I_{D\pm}(\mathbf{x}) = \begin{cases} -1 & \text{if} \quad m(\mathbf{x}) = m^+, \\ +1 & \text{if} \quad m(\mathbf{x}) = m^-. \end{cases}$$

In the examples to follow, we take S^+_{slide} to be the speed of kinesin-5, and S^-_{slide} to be the speed of NCD (values in Table 1). In Sect. 3.3.1, we show results for MT patterning using periodic boundary conditions, and in Sect. 3.3.2, we show results for MT patterning using bounce-back boundary conditions.

3.3.1 Periodic Boundary Conditions

We first simulate our model using periodic boundary conditions, using mixed motor distributions comprised of NCD and kinesin-5 with various motor activities C. Recall that these are the motors used in the gliding assays performed by Tao et al. (2006). The results of Fig. 11a1–a3, show that for low motor activity C, anti-parallel bundles of MTs exist within a disordered MT network. From Fig. 11b1–b3, we see that for higher values of C, a mixed network of MTs exists (there are no apparent anti-parallel bundles). For higher values of C, simulations show similar mixed networks of MTs (results not shown).

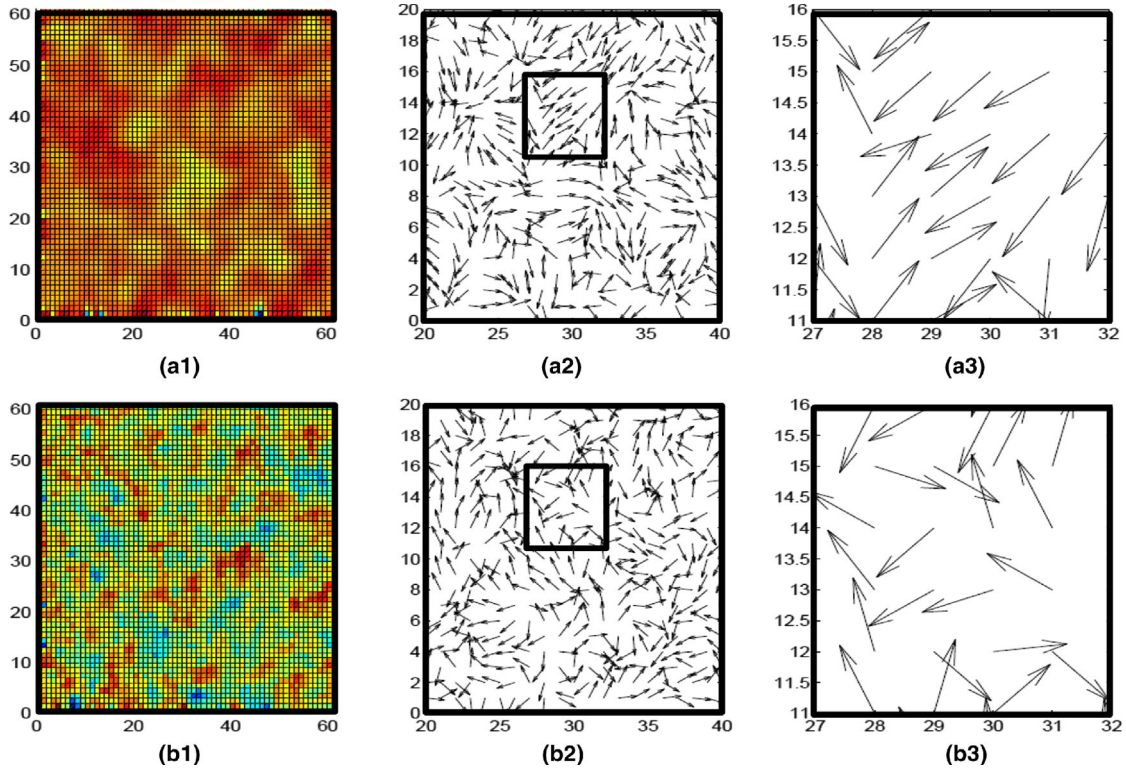

Fig. 11 MT density and mean MT orientation of MTs found after long-time simulation of MTs under the influence of stationary mixed distributions of kinesin-5 and NCD using periodic boundary conditions with (*top*) low motor activity $C = 0.01$ and (*bottom*) higher motor activity $C = 0.5$. *Top*: **a1** MT density shows a mostly uniform distribution of MTs, **a2** MT orientation shows anti-parallel bundles within a mixed orientation of MTs; **a3** Enlarged image of **a2**. *Bottom* **b1** MT density shows patches of MTs; **b2** MT orientation shows a mixed orientation of MTs; **b3** Enlarged image of **a2**. *Red* corresponds to a high density of MTs, while *blue* corresponds to a low density of MTs (Color figure online)

3.3.2 Bounce-Back Boundary Conditions

Next, we show results for kinesin-5 and NCD using bounce-back boundary conditions and varying C. In vivo, such motors help organize MTs into the mitotic spindle in the small constrained domain of the cell, and so here we test what affect the boundary has on MT patterning. The results of Fig. 12a1,b1–a3,b3 show that anti-parallel bundles of MTs exist close to the boundary for low and moderate values of C. For higher values of C, anti-parallel bundles persist (results not shown).

4 Discussion

In this study, we consider the types of MT patterns that can be observed through simulation of the integro-differential Eq. (10) under the influence of either periodic boundary conditions (Eq. 2) or bounce-back boundary conditions (described in Sect. 2.1), describing the evolution of MTs as they interact with stationary distributions of motor proteins. Such an equation describes how MTs organize into complex patterns, by a combination of MT sliding and reorientation in space, due to their interactions with stationary motor proteins.

We first considered the dynamics of MTs under the influence of a single type of stationary motor. Here, we considered motor types that are similar to those that have been studied in previous experiments (Nedéléc et al. 1997; Surrey et al. 2001). For periodic and bounce-back boundary conditions, we tested MT pattern formation for fast plus-end directed motors, similar to the kinesin construct used in Nedéléc et al. (1997), Surrey et al. (2001), as well as a slower minus-end directed motor that is similar to the multimeric NCD construct used in Surrey et al. (2001).

Using periodic boundary conditions and kinesin motors, as we increase the motor activity from low values to high values, we find that the qualitative patterns of MTs change. In particular, we find arrays of vortices for low values of C, we find arrays of asters for moderate values of C , and we find aligned patches (or bundles) for higher values of C. These results are consistent with those of Nedéléc et al. (1997). That is, in the experiments of Nedéléc et al. (1997), vortex patterns were found for small values of motor density, arrays of asters were found for moderate motor densities, and bundles were found Nedéléc et al. (1997) for high motor densities. Recall that the alignment function $\alpha(m)$ is a linear function of m, so that varying C has a similar effect as varying m. Also, in a more recent experiment by Surrey et al. (2001), a transition from vortex patterns to aster patterns was found for increasing motor density.

Using periodic boundary conditions and NCD motors, we find that at low and moderate values of C, asters persist. Also, for high values of C, we found arrays of tight bundles of MTs. These results are also consistent with those of Surrey et al. (2001). That is, for low and moderate values of motor density, asters persist.

It is interesting that we are able to make comparisons with experiments where motors are moving and MTs are dynamic (Nedéléc et al. 1997; Surrey et al. 2001), even though our model treats motors as being stationary. In a newer study, we test the role of dynamic motors on MT patterning (White et al. 2014; Hillen and White 2014). Also, in a future study, it would be interesting to test the role of dynamic MTs (dynamic instability and treadmilling) on MT patterning.

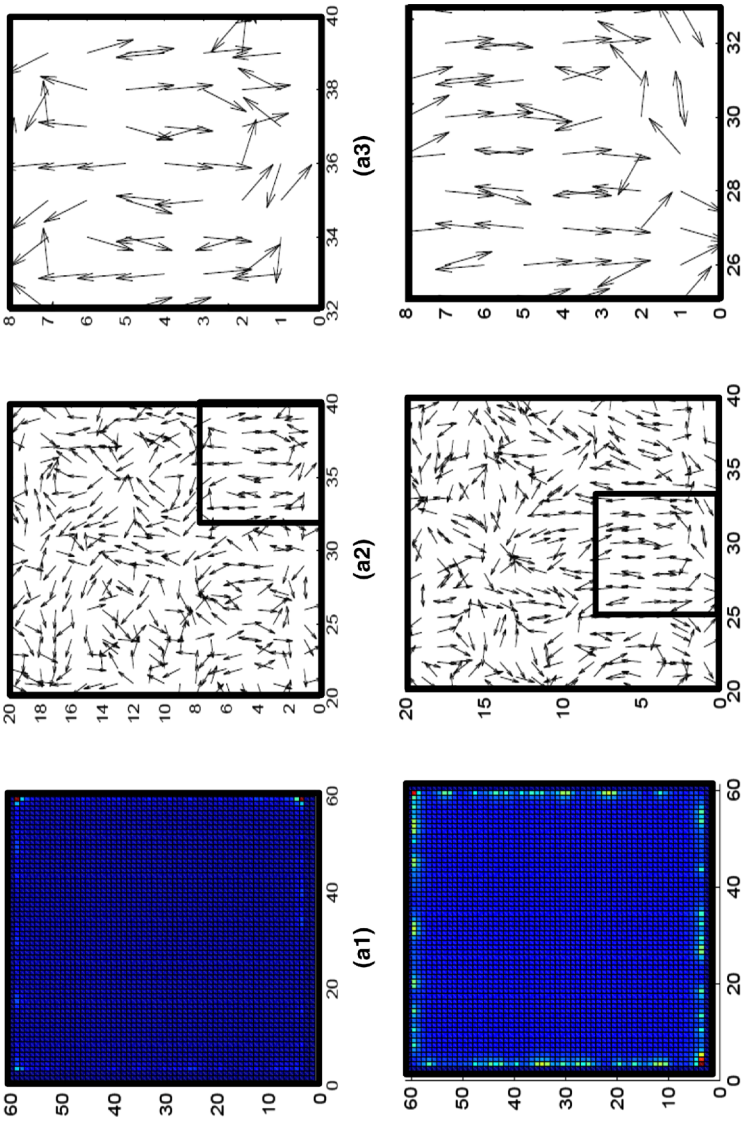

Fig. 12 MT density and mean MT orientation of MTs found after long-time simulation of MTs under the influence of stationary mixed distributions of kinesin-5 and NCD using bounce-back boundary conditions with (*top*) low motor activity $C = 0.01$ and (*bottom*) a higher motor activity $C = 0.5$. *Top* **a1** MT density shows that most MTs end up on the boundary (in the corners mostly); **a2** MT orientation shows anti-parallel bundles close to the boundary; **a3** Enlarged image of **a2**. *Bottom* **b1** MT density shows small uniform density of MTs in the center of domain with most MTs on boundary; **b2** MT orientation shows anti-parallel bundles close to boundary; **b3** Enlarged image of **b2**. *Red* corresponds to a high density of MTs, while *blue* corresponds to a low density of MTs (Color figure online)

Using bounce-back boundary conditions results in vortex patterns for both motors at moderate values of C. However, at low C, kinesin forms a global aster. In the experiments of Nedéléc et al. (1997), for MTs that are stabilized by taxol, motors organize MTs into a global aster. However, in these experiments, when MTs are dynamic (not stabilized by taxol), and when they are placed in constrained domains (domains of various shapes), MTs first form an aster pattern, but later, after coming in contact with the boundary, break down into a vortex pattern. Our simulations suggest that for most values of C, and in small domains, MTs form similar vortex patterns.

After considering MT patterning with one motor type, we studied MT patterning with two motor types. We do this because anti-parallel bundles have been observed in previous experiments involving two motors of opposing directionality (Vale et al. 1992; Hentrich and Surrey 2010; Tao et al. 2006). However, these anti-parallel bundles are not stable, breaking down quickly after they form. These experiments were performed to determine how the overlap of anti-parallel MTs in the mitotic spindle are formed. Also, in vivo, anti-parallel bundles form in the mitotic spindle as a cell prepares to divide. It is believed that the slow-moving, plus-end directed motor kinesin-5, as well as the opposing minus-end directed motor NCD, act between overlapping MTs to form these anti-parallel arrays (Tao et al. 2006; Sharp et al. 2000).

By running simulations with kinesin-5 and NCD motor types, and using both types of boundary conditions, we found that for low values of C, MTs are able to form stable anti-parallel bundles. Using bounce-back boundary conditions, the majority of the anti-parallel bundles are located close to the boundary, whereas using periodic boundary conditions, the anti-parallel bundles are mixed throughout the entire domain. For moderate values of C, we find similar results for bounce-back boundary conditions. However, more MTs are located at the boundary than in the previous case. Also, using periodic boundary conditions, we do not find anti-parallel MTs for moderate C values. Instead, we find mixed arrays of MTs (it is unclear whether stable anti-parallel bundles form). From the previous experiment of Tao et al. (2006), where the motors kinesin-5 and NCD have been studied, it is proposed (from loss-of-function experiments) that the anti-parallel bundles are a result of the balanced activities of the motors moving in opposite direction. However, in the experiment of Tao et al., anti-parallel bundles have not formed stabilized anti-parallel bundles (just transient anti-parallel bundles). From our results, we predict that this could be because the domain was too large and the motor activity was too high. In particular, from our results, anti-parallel bundles will form in any domain if the motor activity C is low, but will always form in closed domains for any value of C (low to high).

By simulation of a mathematical model for MT evolution in the presence of static distributions of motor proteins, a number of interesting patterns that have analogs in both in vivo and in vitro experiments have been found. In particular, patterns such as vortices, asters, parallel, and anti-parallel bundles, arise. Such patterns are dependent on the particular properties of the motors, as well as the motor distributions. In future studies, it would be interesting to look at the effect of higher sliding speeds on MT distributions. Here, we were unable to use higher sliding speeds due to the choice in our numerical scheme (an explicit upwinding scheme). In particular, for our simulations, the sliding speed in a particular direction could not exceed a value consistent with $0.7\,\mu$m/s (so that the Courant number would not exceed the allowed value of 1). This was a suitable restriction for the motor types explored in this paper. However, some motor proteins can move much more quickly. For example, cytoplasmic dynein can move up to speeds of

1.2 μm/s (Howard 2001). Testing MT patterning in the presence of similarly fast motors would require an implicit-type scheme, and is left for future work. In addition, we only considered stationary motor proteins in this paper. In a new study, we explicitly incorporate motor kinetics such as movement along MTs and diffusion in the cytoplasm (White et al. 2014; Hillen and White 2014). Such a model allows us to quantify kinetic properties of motor proteins and study their effect on MT pattern formation.

References

Aranson I, Tsimring L (2006) Theory of self-assembly of microtubules and motors. Phys Rev E 74(3):031915

Dogterom M, Surrey T (2013) Microtubule organization in vitro. Curr Opin Cell Biol 25:23–29

Gibbons F, Chauwin J-F, Despósito M, José J (2001) A dynamical model of kinesin-microtubule motility assays. Biophys J 80:2515–2526

Hentrich C, Surrey T (2010) Microtubule organization by the antagonistic mitotic motors kinesin-5 and kinesin-14. J Cell Biol 189(3):465–480

Hillen T (2006) M5 mesoscopic and macroscopic models for mesenchymal motion. J Math Biol 53:585–615

Hillen T, White D (2014) Existence and uniqueness for a coupled PDE model for motor induced microtubule organization. Submitted to SIAM J Appl Math

Howard J (2001) Mechanics of motor proteins and the cytoskeleton. Sinauer, Sunderland

Humphrey D, Duggan C, Saha D, Smith D, Ka J (2002) Active fluidization of polymer networks through molecular motors. Lett Nat 416:413–416

Janson M, Loughlin R, Loiodice I, Fu C, Brunner D, Nedelec F, Tran P (2007) Crosslinkers and motors organize dynamic microtubules to form stable bipolar arrays in fission yeast. Cell 128:357–368

Jia Z, Karpeev D, Aranson I, Bates P (2008) Simulation studies of self-organization of microtubules and molecular motors. Phys Rev E 77:051905

Karp G (1996) Cell Mol Biol. Wiley, New York

Kim J, Park Y, Kahng B, Lee HY (2003) Self-organized patterns in mixtures of microtubules and motor proteins. J Korean Phys Soc 42(1):162–166

Kirschner M, Mitchison K (1984) Dynamic instability of microtubule growth. Nature 312:237–242

Lee HY, Kardar M (2001) Macroscopic equations for pattern formation in mixtures of microtubules and molecular motors. Am Phys Soc 64:056113

Luo W, Yu C-H, Lieu Z, Allard J, Mogilner A, Sheetz M, Bershadsky A (2013) Analysis of the local organization and dynamics of cellular actin networks. J Cell Biol 202:10571073

Miller C, Ermentrout G, Davidson L (2012) Rotational model for actin filament alignment by myosin. J Theor Biol 300:344359

Mitchison K, Kirschner M (1986) Beyond self-assembly: from microtubules to morphogenesis. Cell 45:329–342

Nedéléc F, Surrey T (2001) Dynamics of microtubule aster formation by motor complexes. Phys Scale Cell 4:841–847

Nedéléc F, Surrey T, Maggs AC, Leibler S (1997) Self-organization of microtubules and motors. Nature 389:305–308

Othmer H (2010) Notes on space- and velocity-jump models of biological movement. Theor Biol 10:913–917

Othmer H, Dunbar S, Alt W (1988) Models of dispersal in biological systems. J Math Biol 26:263–298

Perthame B (2007) Transport equations in biology. Birkhäuser, Berlin

Porter D (1990) Integral equations: a practical treatment from spectral theory to applications. Cambridge University Press, Cambridge

Reymann A-C, Martiel J-L, Cambier T, Blanchoin L, Boujemaa-Paterski R, Théry M (2010) Nucleation geometry governs ordered actin network structures. Nat Mater 9:827–832

Sharp D, Rogers G, Scholey J (2000) Microtubule motors in mitosis. Nature 407:41–47

Smith D, Ziebert F, Humphrey D, Duggan C, Steinbeck M, Zimmermann W, Ka J (2007) Molecular motor-induced instabilities and cross linkers determine biopolymer organization. Biophys J 93:44454452

Surrey T, Nedéléc F, Leibler S, Karsenti E (2001) Physical properties determining self-organization of motors and microtubules. Science 292:1167–1171

Tao L, Mogliner A, Civelekoglu-Scholey G, Wollman R, Evans J, Stahlberg H, Scholey J (2006) A homotetrameric kinesin-5, KLP61F, bundles microtubules and antagonizes Ncd in motility assays. Curr Biol 16:2293–2302

Vale R, Malik F, Brown D (1992) Directional instability of microtubule transport in the presence of kinesin and dynein, two opposite polarity motor proteins. J Cell Biol 119:1589–1596

Vignaud T, Blanchoin L, Thery M (2001) Directed cytoskeleton self-organization. Synth Cell Biol 22:671–682

Wade R (2009) On and around microtubules: an overview. Mol Biotechnol 43:177–191

Waterman-Storer C, Salmon E (1997) Microtubule dynamics: treadmilling comes around again. Curr Biol 7:369–372

Waterman-Storer C, Salmon E (1999) Microtubules: strange polymers inside the cell. Bioelectrochem Bioenerg 48:285–295

White D, de Vries G, Martin J, Dawes A (2014) Microtubule patterning in the presence of moving motors. In preparation

Yokota E, Sonobe S, Igarashi H, Shimmen T (1995) Plant microtubules can be translocated by a dynein ATPase from sea urchin in vitro. Plant Cell Physiol 36(8):1563–1569

Yuko M-K (2001) Shaping microtubules into diverse patterns: molecular connections for setting up both ends. Cytoskeleton 68:603–618

Zhou J, Giannakakou P (2005) Targeting microtubules for cancer chemotherapy. Curr Med Chem 5:65–71